STUDY ON PULSAR EMISSION AND RELATED ISSUES

G.J. QIAO, H.G. WANG, Y.Q. XUE, R.X. XU, K.J. LEE
Peking University, 100871 Beijing, China
gjq@bac.pku.edu.cn

Pulsar radio and gamma-ray emission have been studied for about three decades, but we still lack an elaborated model to account for the emission from radio to gamma-rays at the same time. A joint model for pulsar radio and gamma-ray emission is introduced in this paper. The ingredients of this model are the inverse Compton scattering (ICS) model[1,2,3](hereafter papers I,II,III) for radio emission and a mechanism combined with inner and outer accelerators for gamma-ray emission. In this model both radio and gamma-ray emission beams can be calculated, the core and conal emission beams at radio band are natural results. Various kind of radio and gamma-ray pulse profiles are reproduced, the Geminga-like, Crab-like and Vela-like relative phase between their radio and gamma-ray pulses can also be reproduced. Some other related studies, such as the evidence for outer-gap emission from the X-ray pulsar PSR B1937+21, the death line on $P - \dot{P}$ diagram, a fossil disk around the so called "free precession" neutron star are also discussed.

1 Introduction

More than 1,300 rotation-powered pulsars have been discovered so far, among which seven are gamma-ray pulsars. The abundant observational properties of pulsar emission provide us valuable clues to understand the physics process in pulsar magnetosphere. Below we first summarize the main properties for radio and Gamma-ray emission of pulsars.

Radio

(1) The radio emission beams of pulsars can be divided into two kinds of components, i.e. the core and cone[4], or three kinds, i.e. the core, inner and outer cone[5]. (2) The core and conal components are emitted at different heights. (3) The shapes of pulse profiles change with observing frequencies. (4) The radio emission is generally highly linearly polarized over all longitudes of profiles, but some pulsars may show depolarization and position angle jumps in the integrated profiles. For some pulsars, the position angle sweep is in an "S" shape. The sense of the circular polarization may reverse near the central phase of the integrated pulse. The debate between the "core-cone" beam structure and the "patchy" beam picture has persisted for a long time[6,7,8]. It is possible that the real pulsar emission beam is the convolution of a "patchy" source function and a "window" function[9]. The latter may itself be composed of a central core component plus one or more nested "conal" components.

Gamma-ray (1) The Gamma-ray light curves of most high-energy pulsars show two major peaks which are widely separated ($\sim 20\% - 40\%$ rotational period). (2) Except the Crab pulsar, the other gamma-ray pulsars show significant phase offset between radio and gamma-ray pulses (not including the Geminga pulsar for its radio emission has not be confirmed). (3) The Gamma-ray spectra generally show a cutoff above several GeV. (4) The spectra vary with rotational phase. (5) the Gamma-ray luminosity scales with the particle flux from the open field regions of the magnetosphere.

By now most theoretical models that explain pulsar radio emission are based on the picture of inner vacuum gap, e.g. the inverse Compton scattering model[1,2,3], the spark model[10,11] and plasma emission model[12].

To explain the gamma-ray emission properties, the polar gap (PC) model and the outer gap (OG) models are developed. But there are few efforts to establish a joint model for radio and gamma-ray emission of pulsars. In this paper we present our recent study on such a kind of model. In this model both the inner and the outer accelerators are joined and the radio and Gamma-ray emission properties can be calculated.

The radio emission is produced above the polar cap at different heights for different components (core or cones), while the gamma-ray emission originates at the places near the null charge surface, but the location is different from the conventional CHR outer gap model[13].

In section 2 the ICS model for radio emission is introduced, which is an ingredient of the joint model. In section 3 then we present the basic picture of the joint model for gamma-ray emission. Some related studies we have done, such as the evidence for outer-gap emission from the X-ray pulsar PSR B1937+21, the death line on $P - \dot{P}$ diagram, a fossil disk around the so called "free precession" neutron star are introduced in sections 4-6, respectively.

2 Radio Emission in the ICS Model

The basic picture of the ICS model[1,14] is: low-frequency electromagnetic waves (with frequency $\sim 10^{5-6}$Hz) are assumed to be excited near the pulsar polar cap region by the periodic breakdown of the inner gap and to propagate outwards in the open field line area. These low energy photons are inverse Compton scattered by the secondary particles produced in the pair cascades, and the up-scattered radio photons just provide the observed radio emission from the pulsar.

Fundamental assumptions

The inner vacuum gap model was proposed by Ruderman & Sutherland in 1975 (hereafter RS model) to explain pulsar radio emission. If the ion binding energy on the neutron star surface is large enough, a vacuum gap in the polar cap region could be formed, namely, the inner gap. The RS model can account for some features observed in radio pulsars, such as sub-pulse drifting, microstructure, etc., and is supported by some recent observations[15].

If such a RS-type gap does exist, its periodical breakdown due to pair formation avalanche can naturally provide the low-frequency electromagnetic waves required in the ICS model. However, the RS model confronts the basic difficulty known as the "binding energy problem"[16]. Recent investigations suggest that the inner vacuum gap can be formed in either neutron stars (or crusted strange stars) with extremely strong surface magnetic field ($\sim 10^{13}$G)[17] or bare strange stars[18]. Björnsson (1996) pointed out that if ions are not bound, the outflow current is still not steady unless averaged over a sufficiently long time, since micro-instabilities should exist. Such micro-instabilities make the inner accelerator to show some features similar to what a RS-type vacuum gap shows, and the low frequency waves may also be excited.

On a conventional view, the propagation of the low frequency waves may be prohibited by the dense plasma in pulsar magnetosphere. However, we note that the periodically breakdown of the gap causes the secondary plasma to eject in clumps so that a large space between adjacent clumps is analogous to a vacuum to allow low frequency waves to propagate, at least at low altitudes. Furthermore, owing to that the amplitude of the low frequency wave is very high, nonlinear effects could take a prominent role. In this case, the plasma frequency could be much lower[20], and the low frequency wave can propagate near the neutron star surface. In this paper, we assume that low frequency wave can propagate to the reasonable heights of interest.

"Beam-frequency figure" in the ICS model

The fundamental output of the ICS model is the so-called "beam-frequency figure" or "beaming figure". Fig.1a,b are typical beam-frequency figures of the ICS model (see also Fig.6 in Paper 1). It shows that along a certain field line, when the beaming angle (the angle between the radiation direction and the magnetic axis) increases (the emission altitude gets higher effectively), the emission frequency will decrease sharply from a high level at

first, then rise again after reaching a minimum, and finally drop again after a maximum. Thus if an observer is observing at a certain frequency ν, and if the line-of-sight (hereafter LOS) of the observer is very close to the center of the beams, i.e. the impact angle is very small, all three emission regions, which correspond to the core, inner and outer conal emission respectively, can be observed. Hereafter, the three branches of the beam-frequency figure are referred to as the "core branch", the "inner conal branch" and the "outer conal branch", respectively. Even if observing at a given frequency ν, different observers with different impact angles will look at distinct emission branches so that various pulse profiles are observed.

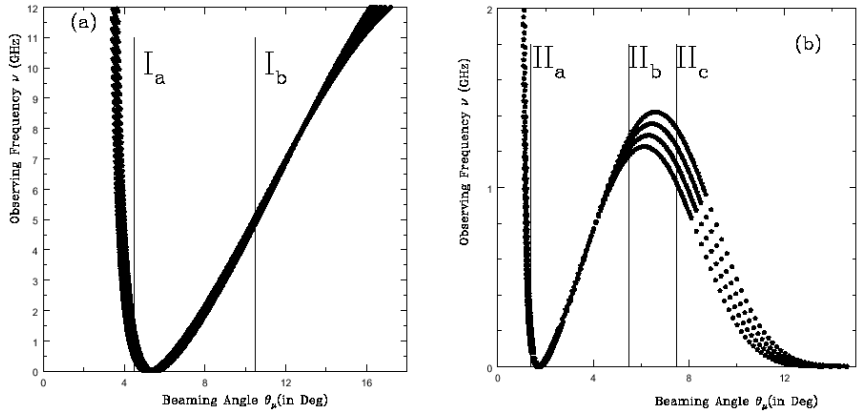

Figure 1. *Two typical "beam-frequency figures" in the ICS model. The observing frequency is plotted versus the so-called beaming angle, the angle between the radiation direction and the magnetic axis. (a) For type I, the lines of a and b correspond to sub-types Ia and Ib. (b) For type II, the lines of a, b, and c correspond to the sub-types of IIa, IIb, and IIc.*

Physically, the shape of the beam-frequency figure is just due to the frequency formula of the ICS mechanism under the condition $B \ll B_{\rm q}$ and $\gamma\hbar\omega_0 \ll m_{\rm e}c^2$, which reads

$$\nu \simeq 2\gamma^2\nu_0(1-\beta\cos\theta_{\rm i}), \tag{1}$$

where $B_{\rm q} = 4.414 \times 10^{13}$G is the critical magnetic field, ν is the scattered frequency, ν_0 is the frequency of the incident low frequency wave, $\beta = v/c$ is the velocity of the secondary particles in unit of light velocity c, $\gamma = 1/(1-\beta^2)^{1/2}$ is the Lorentz factor of the particles, and $\theta_{\rm i}$ is the incident angle (the angle between the direction of a particle and an incoming photon). The Lorentz factor shows a decreasing behavior above the gap due to the energy

loss of the particles. Commonly we assume $\gamma = \gamma_0 \exp[-\xi(r-R)]$, where γ_0 is the initial Lorentz factor of the particles, R is the radius of the neutron star, $r - R$ is the emission height from the neutron star surface, and ξ reflects the scale factor of the deceleration. To obtain the figure, a dipolar magnetic field is assumed.

2.1 The frequency evolution of the integrated pulse profiles

Based on the model results, the frequency behavior of pulsar integrated profiles can be classified as two general types. The first type is the core-dominant pulsar, which only has the core and the inner conal branches in the pulsar beam (Fig.1a). This usually takes place in the short period pulsars. The absence of the outer conal branch is either due to the fact that the deceleration of the pairs is not effective or due to the fact that the low frequency wave may not propagate to higher altitudes. The second type is the conal-dominant pulsar, which have all three branches in the pulsar beam (Fig.1b). This usually occurs in long period pulsars.

As the impact angle gradually increases, pulsars of type I (II) can be further grouped into two (three) sub-types, which show different frequency behavior.

(1) Pulsars of Type Ia have very small impact angles. They normally show single pulse profiles at low frequencies but become triple profiles at high frequencies when the LOS begins to sweep across the inner conal branch. The typical pulsar of this type is PSR B1933+16[4].

(2) Pulsars of Type Ib have larger impact angles than those of type Ia. Though at low frequencies the pulsars show core-triple profiles, they will evolve to conal-double profiles at higher frequencies, when the LOS misses the core branch. The examples of Type Ib are PSR B1845-01[21] and B1508+55[22].

(3) Pulsars of Type IIa have five components at most observing frequencies, since the small impact angle makes the LOS cut through all three branches. A very important feature is that the five pulse components will merge into three components at very low frequencies (see Fig.4 in paper II), which has indeed been observed from some pulsars, e.g. PSR B1237+25[23].

(4) Pulsars of Type IIb, with a larger impact angle, show three components at low observing frequencies, then evolve to four components when frequency is higher, and finally merge to double pulse profiles at the highest frequency. An example is PSR B2045-16[21].

(5) Pulsars of Type IIc have the largest impact angle, so that only the outer conal branch is cut by the LOS. The pulse profiles of this type are

conal double at all observing frequencies, with the separation between the two components decreasing at higher frequencies. Many pulsars belong to Type IIc, such as PSR B0525+21[23], B2020+28[21], PSR B0950+08 [23].

The important features of the ICS model distinguished from the others are two points. First, the angular radius of the inner cone increases at higher frequencies (see Sect. 3.2 of Paper I). Second, the five pulse components will merge into three components at very low frequencies.

In paper II the frequency evolution of the integrated pulse profiles are reproduced with the ICS model for the typical pulsars of each type (see Figs.2-6). The simulations show that the ICS model can well explain the observed multi-frequency profiles of these types of pulsars.

2.2 Linear and circular polarization in ICS Model

The scattered emission by a single relativistic electron in the strong magnetic field is completely linearly polarized, and its polarization position angle is in the co-plane of the out-going photon direction and the magnetic field. However the inverse Compton scattering of a bunch of particles out-flowing in pulsar magnetosphere should be coherent. Such coherence can produce significant circular polarization in beamed radio emission.

In paper III the coherent ICS process in pulsar magnetosphere is simulated. An observer can only see a small part of an emission beam radiated by a particle bunch, which is called as "transient beam". (1) In the ICS model, at a given frequency the transient beam has three parts (core, inner and outer cones), each of them is called "mini-beam", and their polarization features are quite different. (2) Circular polarization is very strong (even up to 100%) in the core mini-beam and it is much less in the inner cone mini-beam. (3) If the LOS sweeps across the center of a core (or inner conal) mini-beam, the circular polarization will experience a central sense reversing, otherwise it will be dominated by one sense, either the left hand or the right hand according to its traversing line relative to the mini-beam. (4) The position angles at a given longitude of transient "sub-pulses" have diverse values around the projection of the magnetic field. The variation range of position angles is larger for core emission, but smaller for conal beam. (5) Stronger circular polarization should be observed in sub-pulses with higher time resolution according to our model.

Fig.2 shows a typical integrated polarization profile calculated by summing up incoherently the Stokes parameters of the scattered waves from the

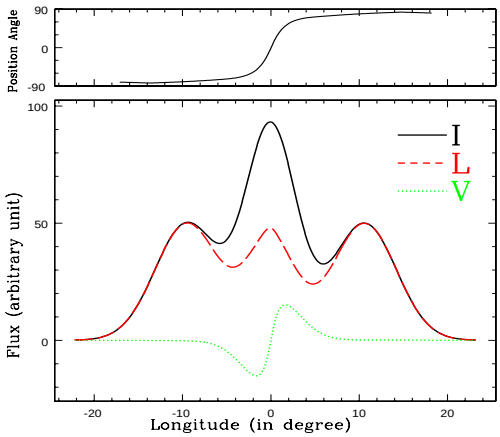

Figure 2. The integrated pulse profile simulated for the normalized impact angle 0.15 (see Paper III for details). An S-shaped position angle swing, the linear polarization, an antisymmetric type of net circular polarization, and a substantial amount of unpolarized emission can be reproduced from the ICS model. A small beam shift between core and conal components due to different emission heights has been included in the simulation.

particle bunches. It is found that the integrated profiles are highly linear polarized in general, and their polarization angles follow nice S-shapes, which represents well the rotating vector model. One important result is the antisymmetric circular polarization in the central or core component.

There is also depolarization in the integrated profiles. As we mentioned before, circular polarization can be up to 100% on some part of core mini-beam (sub-pulses), but depolarization occurs in the process of incoherent summation of circular polarization of opposite senses. This also produces a substantial amount of un-polarized emission. For the linearly polarized emission, position angles of transient sub-pulses vary, causing further depolarization. However, in the conal components, circular polarization is insignificant, mainly because it is originally weak in the mini-beam. Since there is negligible variation of position angles of sub-pulse, almost no linear depolarization presents, and therefore, the conal components are always highly linearly polarized. Considering the retardation effect due to relative phase shift between pulsar beam components, we find that such shift could cause further depolarization and may result in position angle jump in integrated profiles.

3 Gamma-ray Emission from Pulsars in an Joint Model

To reproduce the gamma-ray emission, we assume that there is a second acceleration region near the null charge surface, and the pairs streaming outwards from the inner vacuum gap scatter the low energy photons to gamma-ray photons[24,25].

The scattering happens at the point with distance $r = \lambda R_{\rm null}$ from the center of the neutron star, where the $R_{\rm null}$ is the minimum distance from the stellar center to the intersection of null charge surface and the last open field, λ is a constant which is supposed to be 0.8 in this paper.

Assuming a dipolar magnetic field, the emission location could be given by

$$\theta_{\rm e} = \sin^{-1}\left\{\sqrt{\lambda}\sin\left[\frac{1}{2}\left(\cos^{-1}(-\frac{\cos\alpha}{3}) - \alpha\right)\right]\right\}, \tag{2}$$

where $\theta_{\rm e}$ is the angle between the magnetic axis and the line joining up the stellar center and the emission location, α is the inclination angle between the rotation and magnetic axes. The angle between the radiation direction and the magnetic axis, θ_μ, is given by:

$$\theta_\mu = \frac{\pi}{2} - \alpha - \tan^{-1}\left[\frac{\cos\alpha + 3\cos(\alpha + 2\theta_{\rm e})}{\sin\alpha + 3\sin(\alpha + 2\theta_{\rm e})}\right]. \tag{3}$$

Then the phase separation between two peaks, $\Delta\phi$, can be derived from the following relation[4,26],

$$\sin^2(\theta_\mu/2) = \sin^2(\Delta\phi/4)\sin\alpha\sin(\alpha+\beta) + \sin^2(\beta/2), \tag{4}$$

where β is the impact angle. Supposing that each emission component is Gaussian, we calculate and fit the observed Gamma-ray and radio mean pulse profiles for seven gamma-ray pulsars, as shown in Fig.3.

The above results show that our joint model is advantageous to explain the gamma-ray light curves of pulsars and the relative phase of radio and gamma-ray pulses. More detailed works, such as the phase resolved spectrum at gamma-rays, X-ray emission from pulsars, and so on, are necessary to be investigated latter.

4 Radio and X-ray Emission from PSR B1937+21

A preliminary work we have done on X-ray pulsars is about the origin of the nonthermal X-ray emission from PSR B1937+21[27], the fastest millisecond

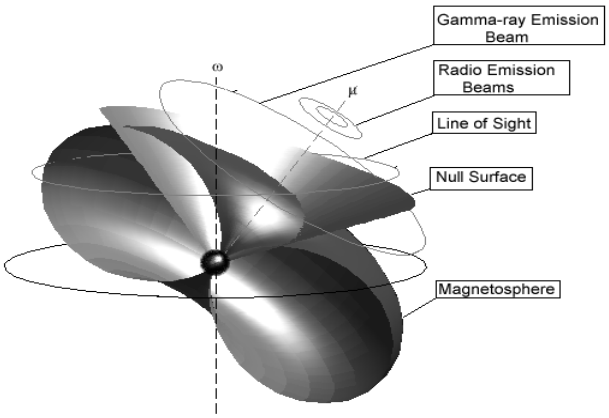

Figure 3. The schematic diagram for pulsar magnetosphere, null charge surface and emission beams. It is shown that the gamma-ray beam can be rather wide with the emission location inside the null charge surface.

pulsar (MSP) discovered so far. This pulsar is unique in X-ray pulsars for its narrow radio and X-ray pulses. The recently observed relative phase between radio and X-ray pulses makes it possible to study the origin of the X-ray emission, namely, to find out whether it is from the polar cap accelerator or the outer-gap accelerator. The approach we used is to model the radio and X-ray profiles in the frames of PC and OG models to find out which model can fit the main observational properties

The main observational facts are summarized as follows. (1) The radio integrated profile is composed of a main pulse and an interpulse, which are separated from each other by a phase of 174° (at 1.4 GHz)[28]. (2) The 10% widths of the radio main pulse and the interpulse are 19.4° and 17.7°, respectively (1.5 GHz, EPN data). (3) The ASCA observations detected only one nonthermal X-ray pulse, which is coincident with the radio interpulse in phase within the timing errors, with a width[28] of 23°.

We made the simplest assumptions that the radio beams from both polar regions have the same width, and the emission pattern in the beams is symmetrical about the magnetic axis. In the PC model these are also assumed for the X-ray beams. In this case, a single X-ray pulse and double radio pulses can be reproduced, but the X-ray pulse is always coincident with the radio main pulse, not the interpulse.

In the latest version of the three-dimensional outer gap model[29], three dimensional scales of the OG are limited by the pair production process in the gap. The emission beam of OG is a fan-like beam, not a hollow cone as in the PC model. Taking an group of reasonable parameters, it is found that the OG model can reproduce the narrow X-ray pulse width, the radio pulse widths, and the coincidence between the X-ray pulse and the radio interpulse, which are in good agreement with the observational data.

General to speak, in the simplest cases the X-ray emission of PSR B1937+21 is more likely from the outer gap. But it should be pointed out that possible significant deviation from the simplest assumptions may exist, and the PC model may be able to explain the observation as well. There may be two kinds of special cases. (1) As to the radio emission, when the pulsar has a non-dipolar magnetic field, the distribution of emission intensity in the radio beams may be different from each other, which could lead to a consequence that for one beam only a part of it is observed while for the other a larger part or the whole is observed. (2) When PSR B1937+21 is a neutron star or a strange star with crust and its inclination angle is near 90^{o}, the X-ray emission pattern may be significantly asymmetric about the magnetic axis, because the two halves of the polar region may be filled with positive ions and electrons, respectively. The ions are less effectively to be accelerated to relativistic energy to radiate high energy emission. Therefore, only single X-ray peak is observed which may be coincident with the radio interpulse. But if the pulsar is a bare strange star, the positively charged half is filled with positrons, so that the X-ray beams should still be symmetrical.

Further research on pulsar magnetosphere structure and emission mechanisms will be helpful to understand the origin of the X-rays for PSR B1937+21. We are expecting that future polarization observations could provide a more confirmative value of the maximum rate of the position angle, which is meaningful not only for constraining whether this pulsar is an NS or an SS but also for a better understanding of its X-ray emission.

5 A New Death Line for Radio Pulsars

Electron-positron pair formation is the essential condition of coherent pulsar radio emission. The condition that pair production is prohibited defines the condition of radio pulsar death. The newly-discovered long-period radio pulsar PSR J2144-3933 ($P = 8.51$s)[30] challenges the present radio emission theories because it seems to be located at the "radio-quiet" region in the $P - \dot{P}$ diagram. Although many authors have investigated the death line for

radio pulsars before and after this discovery[31,32,33], there seems to be not a single death line which can include all the radio pulsars at the "radio-loud" region. We obtained a new death line for radio pulsars within the framework of inner vacuum gap and ICS-induced pair production process, by adopting the criterion that once the possible maximum potential drop in the inner gap is still not enough to produce pairs, the radio emission should not be expected[35].

In the RS model, the particles produced through $\gamma - B$ processes in the gap can be accelerated by the strong electric field parallel to the magnetic field lines and reach very large energy ($\gamma \sim 10^6$). The possible maximum potential drop across the gap is $\triangle V_{\rm max} = (\Omega B/2c) r_{\rm p}^2$, where Ω is the angular frequency of the neutron star, B represents the magnetic field at the surface of the neutron star, $r_{\rm p}$ is the radius of the polar cap. In the inner gap, $\gamma - B$ process plays a very important role. The mean photon free path in strong magnetic field is given by $l = (4.4\hbar^2/e^2 m_{\rm e})(B_{\rm q}/B_\perp)\exp[4/(3\chi)]$, where $\chi \equiv (E_\gamma/2m_{\rm e}c^2)\sin\theta(B/B_{\rm q}) = (E_\gamma/2m_{\rm e}c^2)(B_\perp/B_{\rm q}) \ll 1$[36], $\hbar$ the Planck's constant, $B_\perp \approx hB/\rho \approx lB/\rho$[34] is the magnetic field perpendicular to the moving direction of γ photons (h is the height of the gap, $l \approx h$ is assumed as the condition for the sparks to be produced, $\rho \approx (4/3)(\lambda Rc/\Omega)^{1/2}$ is the curvature radius of the dipole magnetic field lines). The dipolar magnetic field can be written as $B = 3.2 \times 10^{19}(P\dot{P})^{1/2}$ Gauss. When the ICS process plays a dominant role in gamma-ray photon creation in the inner gap, the energy of gamma-rays is $E_\gamma \approx 2\gamma^2\hbar\omega(1 - \beta\cos\theta_{\rm i})$. From the equations above we get a death line (see Fig.4): $1.2 \times 10^{-25} P^{3.5}\dot{P}^{-1.5} = 60.5 + \ln\dot{P} - 2\ln P$ (the field line at $0.8\theta_{\rm p}$ is taken and $l = h = 0.5 r_{\rm p}$ is assumed).

In the $\gamma - B$ process, the magnetic energy density should be high enough. We assume that the perpendicular magnetic energy density is not less than the pair energy density, that is $B_\perp^2/8\pi \geq 2m_{\rm e}c^2 n_{\rm ph}$, where $n_{\rm ph} = (2.4/\pi^2)(kT/\hbar c)^3$ is the number density of photons that produce pairs in the $\gamma - B$ process (when $T = 10^5$ K). Adopting a dipole magnetic configuration and $l = 0.5 r_{\rm p}$, we work out the "appearance line" (see Fig.4): $\log\dot{P} - \log P = -18.7$.

Thus, we have shown a new death line and the appearance line under the inner vacuum gap model without any additional assumptions. Above (below) the death line, neutron stars should be radio-loud (radio-quiet); above (below) the appearance line, pair production process can (cannot) take place, so pulsars there are radio-loud (radio-quiet). The death line and the appearance line in Fig.4 can keep all observed radio pulsars, including the 8.5s pulsar, in

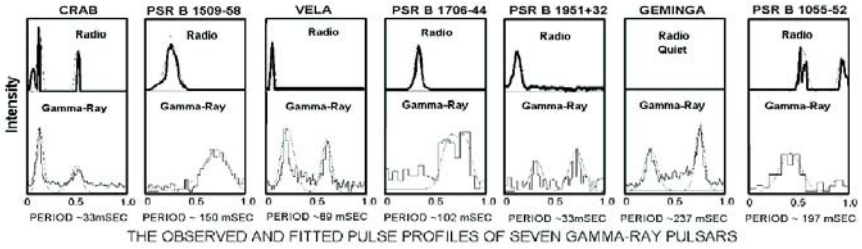

Figure 4. The fitted mean pulse profiles for seven gamma-ray pulsars, where the dash lines are the fitted and the solid lines are the observed profiles.

the radio-loud region.

6 Is There a Fossil Disk Around the So-called Free-Precession Neutron Stars?

The long-term, highly periodic and correlated variations in both the pulse shape and the slow-down rate of two isolated pulsars PSR B1828-11[37] and B1642-03[38] were discovered recently. This phenomenon provides the most compelling evidence for precession. Some authors[39,40] presented different models to explain this phenomenon within the framework of free precession. Recently we proposed an accretion disk model for this precession phenomenon instead[41]. Under reasonable parameters, the observed phenomenon can be explained by an isolated pulsar with a fossil disk.

In our disk-induced precession scenario, the total torque exerted on the pulsar by the fossil disk, which causes the pulsar to precess, is nonzero, due to the asymmetry in pulsar shape (considering the neutron star as a rotation ellipsoid) and nonalignment between the disk rotation axis and the axis of pulsar moment of inertia. For simplicity, we assume the rotation axis is aligned with the principal axis of moment of inertia of the neutron star; in this case, free precession doesn't exist and we can see how the disk makes the neutron star precess more clearly. Below we present the formulae of the gravitational potential in the neutron star-disk system and the angular velocity of neutron

star precession. And then, as an example, we model the precession period of PSR B1818-11. The parameters about PSR B1828-11 are as follows[37]: $P = 0.405$ s, $\dot{P} = 6.0 \times 10^{-14}$ ss^{-1}, $P_{\rm pre} \approx 1000$ days (precession period), $B = 5.0 \times 10^{12}$ G.

The gravitational potential between the neutron star and the disk is

$$V = -\frac{2GMM_0}{c+d}[1 - \frac{b^2+2a^2}{10cd} + \frac{3b^2}{20cd}\sin^2\theta + \frac{3a^2}{20cd}(1+\cos^2\theta)], \qquad (5)$$

where M, a and b are the mass, the equatorial and longitudinal radii of the neutron star, respectively, M_0 is the mass of the disk, c and d are the inner and outer radii of the disk, respectively, θ is one of the three Euler angles (θ, φ and ϕ).

Since the rotation angular velocity of the neutron star ω is much greater than the precession angular velocity of the neutron star $\dot{\phi}$, the angular momentum of the neutron star can be written as $L_0 \simeq I_z\omega$. According to the Lagrange's equation[42]

$$L_0\dot{\phi}\sin\theta = -\partial V/\partial\theta\,, \qquad (6)$$

we have

$$\dot{\phi} = -[3GM_0\cos\theta/(2cd(d+c)\omega)](1 - b^2/a^2)\,. \qquad (7)$$

In terms of the study of the Maclaurin spheroids, we can obtain the oblateness of this pulsar:

$$\epsilon = (a-b)/a = 2.27 \times 10^{-6}\,. \qquad (8)$$

For simplification, we assume $c \approx d \approx R$, so that:

$$\dot{\phi} = -(3GM_0\cos\theta/4R^3\omega)[1 - (1-\epsilon)^2]\,. \qquad (9)$$

According to this equation, we can know the relation between M_0 and R derived from the 1000-day precession period for a group of θ. In principle, M_0 may vary from less than $0.001M_\odot$ to even $0.1M_\odot$, and R from about $1R_{\rm co}$ (or smaller) to $2 \sim 3R_{\rm co}$ when θ varies within the range of $0 \sim 90^{\rm o}$, where $R_{\rm co}$ is the corotation radius of the disk with the pulsar.

We have ignored the angular momentum of the pinned superfluid in the dynamic equations of the calculation. Can the pinning force be strong enough to damp any precession of neutron stars? In principle, detailed computations may determine whether the vortices are pinned, but a definitive conclusion on the nature has not been reached yet due to various uncertainties in the microscopic physics. Nevertheless, Shaham (1986) indicates an unpinned superfluid in the case of precession. It is also noted by Link & Cutler (2002)

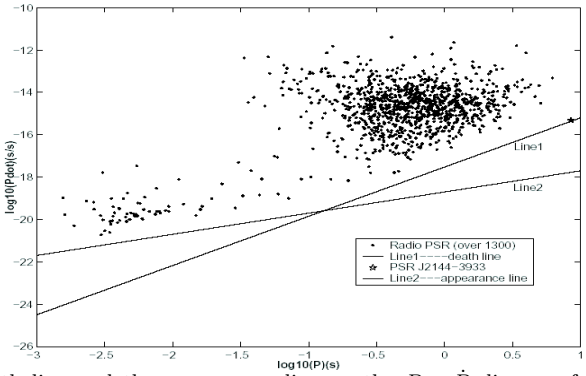

Figure 5. The death line and the appearance line on the $P - \dot{P}$ diagram for over 1,300 pulsars.

that hydrodynamic forces present in a precessing star are probably sufficient to unpin all of the vortices of the inner crust. In addition, the 35-d periodicity of the accreting binary system (Her X-1) has been interpreted as precession[43], which could be another example of forced precessions. We have therefore a tendency to suggest that, the observation of PSR B1828-11 precession may imply that the vertex pinning in this pulsar is much weaker than that predicted previously, at least it is weaker than the possible disk-driven precession effect.

Our accretion disk model for periodic timing variations of pulsars (e.g. PSR B1828-11) can elucidate the observed precession period. If our model proves to be true, the fossil disk model for the anomalous X-ray pulsars may be strengthened. It also presents an indirect evidence for the existence of the fossil disk in nature.

Acknowledgments

This work is supported by National Nature Sciences Foundation of China (10073001 & 10273001).

References

1. Qiao, G.J.& Lin, W.P., A&A, **333**, 172 (1998).
2. Qiao, G.J., Liu, J.F. Zhang, B. & Han, J.L., A&A,**377**,964 (2001).

3. Xu, R.X., Liu, J.F., Han, J.L. & Qiao, G.J. ApJ, **535**, 354 (2000).
4. Lyne, A.G. & Manchester, R.N., MNRAS, **234**, 477 (1988).
5. Rankin, J.M., ApJ, **274**, 333 (1983).
6. Gil, J. A., & Krawczyk, A., MNRAS, **280**, 143 (1996).
7. Han, J.L. & Manchester, R.N., MNRAS, **320**, L35 (2001).
8. Gangadhara, R. T., & Gupta, Y., ApJ, **555**, 31 (2001).
9. Manchester, R.N., J. Astrophys. Astr., **16**, 107 (1995).
10. Gil, J.A. & Sendyk, M., ApJ, **541**, 351 (2000).
11. Melikidze, G.I., Gil, J.A., Pataraya, A.D., ApJ, **544**, 1081 (2000).
12. Melrose, D.B. & Gedalin, M.E., ApJ, **521**, 3511 (999).
13. Cheng, K.S., Ho, C. & Ruderman, M.A., ApJ, **300**, 500 (1986).
14. Qiao, G.J., Vistas Astron., **31**, 393 (1988).
15. Deshpande, A.A. & Rankin, J.M., MNRAS, **322**, 438 (1999).
16. Kössl, D., Wolff, R.G., Miller, E., and Hillerbrandt, W., A&A, **205**, 347 (1988).
17. Gil, J.A. & Melikidze, G.I., ApJ, **577**, 909 (2002).
18. Xu, R.X., Qiao, G.J. & Zhang, B., ApJ, **522**, 109 (1999).
19. Björnsson, C.-I., ApJ, **471**, 321 (1996).
20. Kotsarenko, N.Ya., Stewart, G.A., and Vysloukh, V., Ap&SS, **243**, 427 (1996).
21. Kramer M. et al., A&AS, **107**, 527 (1994).
22. Sieber, W., Reinecke, R., & Wielebiski, R., A&A, **38**, 169 (1975).
23. Phillips, J.A., & Wolszczan, A., ApJ, **385**, 273 (1992).
24. Qiao G.J., Lee K.J., Wang H.G., & Xu R.X., astro-ph/0303231 (2003a).
25. Qiao G.J., Lee K.J., Wang H.G., & Xu R.X., astro-ph/0303232 (2003b).
26. Gil, J., Gronkowski, P. & Rudnicki, W., A&A, **132**, 312 (1984).
27. Wang H.G., Xu R.X. & Qiao G.J., ApJ, **578**, 385 (2002).
28. Takahashi, M. et al., ApJ, **554**, 316 (2001).
29. Cheng, K.S., Ruderman, M.A. & Zhang, L., ApJ, **537**, 964 (2000).
30. Young, M. D., Manchester, R. N., Johnsoton, S., Nature, **400**, 848 (1999).
31. Qiao, G.J. & Zhang, B., A&A, **306**, 5 (1996).
32. Zhang B., Harding A.K. & Muslimov A.G., AAS, 19513303Z (1999).
33. Gil, J., Mitra, D., ApJ, **550**, 383 (2001).
34. Ruderman, M.A. & Sutherland, P.G., ApJ, **196**, 51 (1975).
35. Qiao, G.J., Xue,Y.Q., Zhang, B., Xu, R.X., & Ye, F.F., in IAU Symposium 214, in press (2002).
36. Erber, T., Rev. Mod. Phys., **38**, 626 (1966).
37. Stairs, H., Lyne, A. G., Shemar, S. L., Nature, **406**, 484 (2000).
38. Cordes, J. M., in ASP Conf. Ser. 36, Planets around Pulsars, 43 (1993).
39. Jones, D. I. & Andersson, N., MNRAS, **324**, 811 (2001).

40. Link, B., & Epstein, R. I., ApJ, **556**, 392 (2001).
41. Qiao G.J., Xue Y.Q., Xu R.X., Wang H.G. & Xiao B.W., A&A, submitted (2002).
42. Qiao, G. J., Cheng, J.H., ApJ, **340**, 503 (1989).
43. Shakura, N. I. et al., A&A, **331**, L37 (1998).
44. Shaham, J., ApJ, **310**, 780 (1986).
45. Link, B., Cutler, C., MNRAS, **336**, 211 (2002).